

**Biomimetic Synchronization in Biciliated Robots**

Yiming Xia<sup>1,2,\*</sup> Zixian Hu<sup>1,2,\*</sup> Da Wei<sup>1,†</sup> Ke Chen<sup>1,2,3,‡</sup> Yi Peng<sup>1,2,§</sup> and Mingcheng Yang<sup>1,2,3,||</sup>  
<sup>1</sup>Beijing National Laboratory for Condensed Matter Physics and Laboratory of Soft Matter Physics, Institute of Physics,  
 Chinese Academy of Sciences, Beijing 100190, China

<sup>2</sup>School of Physical Sciences, University of Chinese Academy of Sciences, Beijing 100049, China

<sup>3</sup>Songshan Lake Materials Laboratory, Dongguan, Guangdong 523808, China

 (Received 3 November 2023; revised 15 April 2024; accepted 10 June 2024; published 24 July 2024)

Direct mechanical coupling is known to be critical for establishing synchronization among cilia. However, the actual role of the connections is still elusive—partly because controlled experiments in living samples are challenging. Here, we employ an artificial ciliary system to address this issue. Two cilia are formed by chains of self-propelling robots and anchored to a shared base so that they are purely mechanically coupled. The system mimics biological ciliary beating but allows fine control over the beating dynamics. With different schemes of mechanical coupling, artificial cilia exhibit rich motility patterns. Particularly, their synchronous beating display two distinct modes—analogueous to those observed in *C. reinhardtii*, the biciliated model organism for studying synchronization. Close examination suggests that the system evolves towards the most dissipative mode. Using this guideline in both simulations and experiments, we are able to direct the system into a desired state by altering the modes' respective dissipation. Our results have significant implications in understanding the synchronization of cilia.

DOI: [10.1103/PhysRevLett.133.048302](https://doi.org/10.1103/PhysRevLett.133.048302)

Synchronization is a phenomenon across scales [1]. It means that oscillators unify their rhythm through interactions. In this way, output of individual oscillators can add up and give rise to collective behaviors on a larger scale. Ciliary motility is an archetype of such emergence. A cilium is an active eukaryotic organelle that bends periodically to pump fluid. Synchrony among thousands of beating cilia creates fluid flows on a scale ( $10^{-3}$ – $10^{-1}$  m) orders of magnitude larger than a single cilium ( $10^{-5}$ – $10^{-4}$  m) [2,3]. Microorganisms exploit such flows to swim, and mammals use them to transport fluid [4]. The efficiency of these flows are crucially affected by the exact mode of synchronization (spatial-temporal phase dynamics) [5]. How cilia couple to each other to synchronize and exhibit distinct modes, is a question that has garnered decades of attention [6–9]. In general, the coupling mechanisms fall into two categories. While hydrodynamic interaction is sufficient for some organisms [10–12], direct mechanical connections at the ciliary bases are crucial for others, including the model organism for studying ciliary synchronization, *C. reinhardtii* (CR) [13–15].

So far, our understanding of how mechanical connections help cilia synchronize is still limited [16]. The

limitation arises from two fundamental challenges in experimenting with living samples. First, cilia operate in fluid and are closely spaced such that their hydrodynamic interactions cannot be neglected. Secondly, biomechanical coupling is difficult to isolate from the cell's ongoing physiological and biochemical processes for controlled experiments. An example is that the cilia of CR cells completely fail to synchronize when the cell is demembrated and reactivated *in vitro* [17].

Biomimetic systems in a fluid-free environment provide a possibility to overcome these challenges. Recently, Zheng *et al.* demonstrated that a chain of self-propelling robots can spontaneously oscillate and two bonded chains may even synchronize [18]. The observed oscillation resembles the beating of a biological cilium visually. And in the meantime, it is also overdamped like the latter, i.e., the inertia effects of single robots matter negligibly on the spatial and time scale of the chains' oscillation [18,19].

These findings suggest the biomimetic cilia to be an ideal platform for studying ciliary synchronization exclusively mediated by mechanical connections. Particularly, such systems give an opportunity to elucidate the role of ciliary connections in the emergence of distinct modes of synchrony found in ciliates [15,16,20] and their underlying energetics, which is of fundamental importance but largely unexplored yet.

In this Letter, we devise a biciliated robotic system with the quintessential architecture of a CR cell: two cilia anchored on the same base (body). The base is subjected

\*These authors contributed equally to this letter.

†Contact author: [weida@iphy.ac.cn](mailto:weida@iphy.ac.cn)

‡Contact author: [kechen@iphy.ac.cn](mailto:kechen@iphy.ac.cn)

§Contact author: [pengy@iphy.ac.cn](mailto:pengy@iphy.ac.cn)

||Contact author: [mcyang@iphy.ac.cn](mailto:mcyang@iphy.ac.cn)

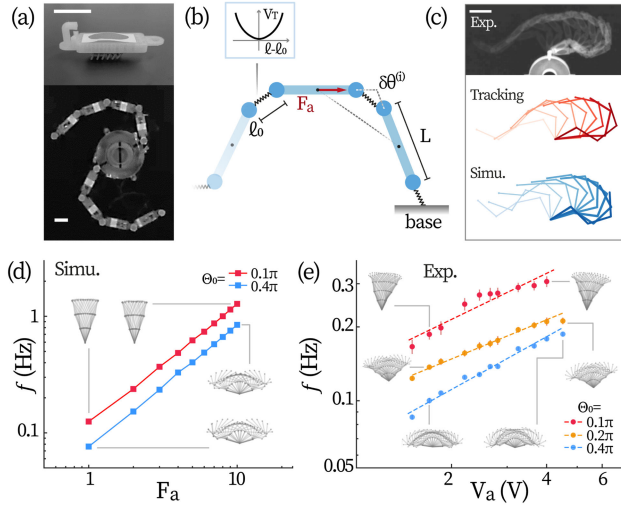


FIG. 1. Experimental and simulation systems. (a) A Hexbug robot with 3D printed cap (upper panel) and two chains each comprising  $N = 4$  robots anchored on a common base (lower panel). Scale bars: 3 cm. (b) The simulation model. (c) Time-lapsed waveform of a single robotic cilium over half a cycle. Frequency and waveform of a single cilium vs the self-propelling force  $F_a$  ( $V_a$ ) for different maximum bending angles  $\Theta_0$ , obtained by simulations (d) and experiments (e). Insets: full-cycle time-lapsed ciliary waveform under the marked conditions.

to designed kinematic constraints. Meanwhile, we develop a simulation model that captures experimental observations accurately. In both experiments and simulations, our system displays both in-phase (IP) and antiphase (AP) mode of synchronous beating that are analogous to those found in CR cells. We reveal that the emergence of and the competition between these modes are governed by the maximization of energy dissipation, i.e., between two possible states, the system favors the one with stronger energy dissipation.

*Experimental and simulation systems*—A robotic cilium consists of a chain of Hexbug (Nano<sup>®</sup>) robots connected end to end by 3D-printed joints. The joints are loose until neighboring units reach an angle of  $\Theta_0$ . The Hexbugs constituting one cilium are powered in parallel by an external dc source with voltage  $V_a$ . When operating, a Hexbug generates vertical vibration at  $\sim 100$  Hz which is converted into self-propulsion by its elastic forward-leaning legs [Fig. 1(a), top panel]. When a chain of Hexbugs is anchored to a base, it oscillates spontaneously due to bifurcation [18,21], displaying waveforms analogous to biological cilia. We anchor two cilia on a shared base [Fig. 1(a) lower panel], which provides direct mechanical coupling between the cilia. Additionally, physical constraints can be integrated into the base to favor either translational or rotational motion [22], helping reveal how basal motion mediates synchronization.

Meanwhile, weights ( $m = 15\text{--}500$  g) are loaded on the base to tune the friction between the base and the surface of

the table, which modulates the strength of mechanical coupling. Ciliary beating is recorded by videography at 46.5 fps from which each robot is tracked with custom PYTHON scripts. From ciliary shapes, we compute observable-independent oscillatory phases of the cilia [25]; and we characterize synchronization by the time fraction of phase-locked beating  $\tau = t_{\text{sync}}/t_{\text{total}}$ , see [22] for the method.

The artificial ciliary system is also studied by means of Brownian dynamics simulations, where each Hexbug is represented as an active rod (length  $L$ ) with a constant self-propelling force  $F_a$  along its long axis [Fig. 1(b)]. Meanwhile, stochastic forces  $\xi_T$  and torques  $\xi_R$  deriving from the environment with temperature  $T$ , are exerted on each robot but not on the base. Neighboring rods are connected by a short harmonic spring between their ends. The ciliary bending angle  $\delta\theta$  is restricted within  $[-\Theta_0, \Theta_0]$ . The translational (rotational) friction coefficients for the Hexbugs and the base are, respectively, denoted as  $\eta_0$  ( $\eta_{0,R}$ ) and  $\eta$  ( $\eta_R$ ). Unless otherwise stated,  $\eta_{(0,R)}/\eta_{(0)} = L^2/12$  is used in simulations [26]. This relation is obtained for a rod-shaped particle in the absence of hydrodynamic interaction. The simulations reproduce the experimental results accurately [Fig. 1(c)]. More details including the modeling scheme, a quantitative correspondence between simulations and experiments, and possible effects of the self-alignment of a single robot, can be found in [22].

The beating of a single cilium is characterized by its cyclic configuration (waveform), frequency ( $f$ ), and the noise in oscillatory phase ( $T_\phi$ ). In our system, the waveform is determined by the number of Hexbugs  $N$  and the maximal bending  $\Theta_0$ . Under given  $N$  and  $\Theta_0$ ,  $f$  is controlled by  $F_a$  ( $V_a$ ); and  $T_\phi$  is derived solely from  $T$ . Notably, in our system, control over waveform and frequency is decoupled, i.e., varying  $F_a$  ( $V_a$ ) does not change the waveform [Figs. 1(d) and 1(e) insets]. This decoupling marks a key difference from the elastically connected chains in Ref. [18], and probably results from the inelastic connection scheme we use. The decoupling is practically advantageous for exploring the parameter space of ciliary beating. In the following, we will focus on robotic cilia formed with  $N = 4$  robots with  $\Theta_0 = 0.4\pi$ .

*Modes of synchronization*—Whether two coupled oscillators can synchronize is primarily determined by the competition between their mismatch in intrinsic frequencies  $\nu = f_1 - f_2$  (detuning) and their coupling strength  $\epsilon$  [1]. Therefore, for studying how two cilia synchronize via a common anchoring base, we examine the system by scanning  $\nu$  and  $\epsilon$ . Practically, we fix the frequency of one cilium ( $F_a = 5$ ,  $V_a = 2.4$  V) and vary that of the other ( $F'_a$ ,  $V'_a$ ) to modulate  $\nu$ . We scan  $\eta$  or  $m$  to control  $\epsilon$ , because  $\epsilon$  is expected to decrease with increasing friction: on a completely fixed ( $\eta, m \rightarrow \infty$ ) base, two cilia will beat completely independently ( $\epsilon = 0$ ). Finally, in experiments, the noise is low and invariant with the driving voltage; while, in simulation, we set one of the cilia as noise free and

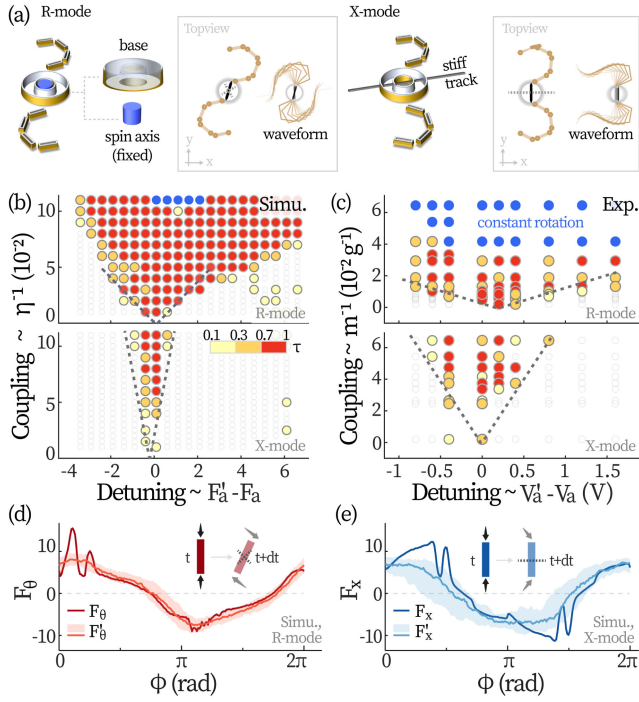


FIG. 2. Synchronization through different basal motion. (a) Experimental schemes (3D) and typical ciliary shapes and synchronous waveforms (boxed) supported by basal rotation (left) and translation in  $x$  (middle). Arnold tongue diagrams for the two modes obtained from simulations (b) and experiments (c). Empty points in the background are measurements where  $\tau < 0.1$ . Dashed lines: boundaries of the synchronization region. Median force waveform over  $\mathcal{O}(10^2)$  synchronized cycles at  $\sim 0$  detuning in  $R$  mode (d) and  $X$  mode (e). Shadings represent interquartile ranges and insets show how cilia can cooperate to maximize basal motion in each mode.

the other one noisy ( $T = 0.8$ ), such that the systems display richer phase dynamics.

We find that the basal rotation and translation promote distinct modes of synchrony [Fig. 2(a)]. When only basal rotation is allowed ( $R$  mode), the synchronous ciliary beating (gait) is analogous to the freestyle swimming, see Supplemental Material Video (SV) 1 [22]. However, when the base is confined to move along the  $x$  axis ( $X$  mode), the supported gait is akin to the breaststroke of a human swimmer (SV 2). Here, the  $x$  axis is perpendicular to the line connecting the two anchoring points on the base. Experimentally, the  $R$  mode and  $X$  mode are realized by integrating a fixed spin axis or a stiff track into the base, see the 3D schematics in Fig. 2(a). Last, basal translation in  $y$  ( $Y$  mode) hardly supports any stable synchronization, and will not be discussed. The “freestyle” and “breaststroke” modes resemble the antiphase and in-phase synchronization observed in CR [15,20,27,28], respectively.

The resultant landscape of synchronization (“Arnold tongues” diagrams) for different basal modes are presented in Figs. 2(b)–2(c). The coupling strength  $\varepsilon$  provided by the

base of given friction can be measured by the phase dynamics described in the Adler equation:

$$\dot{\Delta\phi} = 2\pi\nu - 2\pi\varepsilon \sin \Delta\phi + \zeta(t). \quad (1)$$

Here,  $\Delta\phi = \phi_1 - \phi_2$  denotes the oscillators’ phase difference and  $\zeta(t)$  is the zero-mean Gaussian white noise with  $\langle \zeta(t' + t)\zeta(t') \rangle = 2T_\phi \delta(t)$ . Equation (1) shows that, in the range of detuning  $\nu$  where  $|\nu| \leq |\varepsilon|$ , synchronization can establish. Thus, for a given  $\eta$  ( $m$ ), we approximate  $\varepsilon$  by the width in  $\nu$  where there is synchronization and find empirically that  $\varepsilon \propto \eta^{-1}(m^{-1})$ , see [22] for quantitative conversions. At the given  $\eta$  or  $m$ , we observe that  $\varepsilon_R$  to be much larger than  $\varepsilon_X$  [dashed lines in Figs. 2(b) and 2(c)] for both simulations and experiments. Moreover, Eq. (1) also captures the steady-state phase difference  $\delta\phi = \sin^{-1}(\nu/\varepsilon)$  between synchronized cilia [22].

Although the “freestyle” (in  $R$  mode) and the “breaststroke” (in  $X$  mode) gaits bear distinct appearances, their driving forces exerted by the cilia on the base (i.e., the azimuthal component  $F_\theta$  for the  $R$  mode and the  $x$  component  $F_x$  for the  $X$  mode) actually experience the same in-phase coordination, see Figs. 2(d) and 2(e). The interplay between the ciliary forces sheds light on why  $\varepsilon_R > \varepsilon_X$ . In this system, one cilium exerts force on the base and generates basal motion that influences the beating of the cilium on the other end. In this way, the two cilia interact. Naturally, the larger the transmitted motion is, the stronger the coupling will be. In the  $X$  mode, a given force  $F$  applied at one end generates, per unit time, a displacement of  $F/\eta$  on the other end. However, in the  $R$  mode, the transmitted displacement is much larger ( $3F/\eta$ ), thus consistent with  $\varepsilon_R > \varepsilon_X$ . It bears emphasis that this analysis is qualitative, as coupling strength is expected to be positively associated with, but not necessarily linearly proportional to, the transmitted displacement.

Besides the synchronous beating, when friction of the base  $\eta$  is extremely low, the system in the  $R$  mode evolves into a state of constant rotation [blue bullets in Figs. 2(b) and 2(c)]. In this case, the system persistently rotates in a direction at a uniform speed, with the cilia maintaining a stable configuration. In order to explore other possible dynamic states, we set the cilia to be 10% detuned ( $F'_a = 1.1F_a$ ) and equally noisy ( $T = 0.2$ ), and scan  $F_a$  and  $\eta$  over 3 orders of magnitude in simulations. The system’s complete state diagrams in the  $R$  and  $X$  mode are, respectively, displayed in Figs. 3(a) and 3(b) and they resemble each other qualitatively. The diagrams’ left sides are fluctuation regimes where the noise  $T$  dominates over  $F_a$ . Here, cilia either wiggle without a well-defined frequency (gray) or simply stagnate (dark gray). When  $F_a$  overcomes the noise, as  $\eta$  decreases, two cilia evolve from beating independently (dark purple) to beating synchronously (yellow to red). Eventually, for sufficiently low  $\eta$ , the  $R$  mode and  $X$  mode are, respectively, dominated by

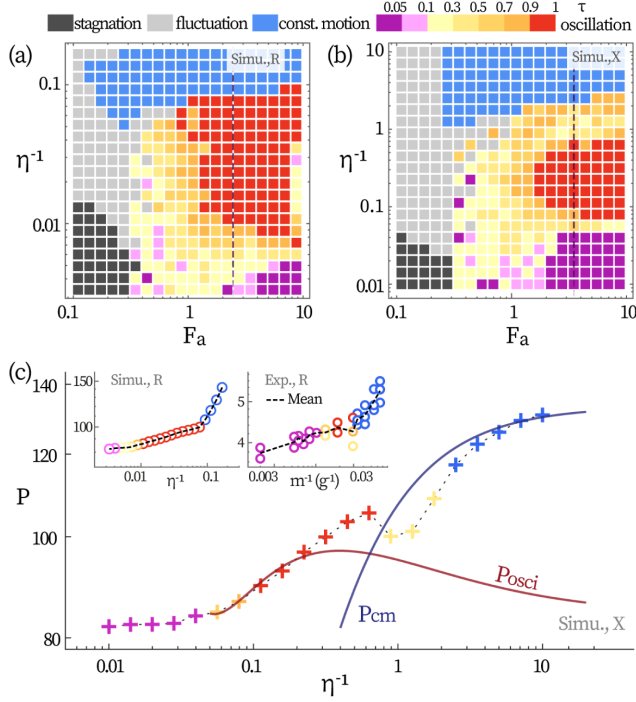


FIG. 3. Dynamic phases of two coupled cilia. Phase diagrams of (a) the  $R$  mode and (b)  $X$  mode obtained from simulations. Vertical dashed lines correspond to the data shown in (c). (c) Typical dissipative power  $P$  as a function of  $\eta$  in the  $X$  mode ( $F_a \approx 3.5$ ).  $P_{\text{cm}}$  and  $P_{\text{osci}}$  are dissipation computed by ciliary shapes displayed in the constant motion and in the oscillation states.  $P$  for  $R$  mode is displayed in left (simulation) and right inset (experiments,  $V_a \approx 2.0$  V).

constant rotation and constant translation (blue). Please see Supplemental Material, SV 3–SV 5 for the mentioned states and [22] for how they are quantitatively labeled.

**Energetics**—Such rich state diagrams naturally raise a question: energetically, what determines the stability of these states and their intertransitions? Inspired by previous studies [9,29] that revealed a positive association between oscillators’ coupling strength and energy dissipation, we examine how dissipation is involved in the system’s evolution. We find that, between two possible states, the system will evolve into the more dissipative one, as demonstrated below.

The system’s dissipation is computed as  $P = \langle \sum_i (\mathbf{F}_i \cdot \mathbf{v}_i + M_i \omega_i) \rangle$  [30]. The subscript  $i$  ranges over all robot units and the base;  $\mathbf{v}$  and  $\omega$  denote velocity and angular velocity, respectively. For details see [22]. Representative traces of  $P$  underlying the transition from oscillation to constant motion are displayed in Fig. 3(c) [corresponding to the vertical dashed lines in Fig. 3(b)]. Overlaid on the system’s actual dissipation  $P$  are the estimated dissipation of ciliary oscillations  $P_{\text{osci}}$  and that of constant motion  $P_{\text{cm}}$  [22]. Clearly, when constant motion becomes more dissipative ( $P_{\text{cm}} > P_{\text{osci}}$ ), it replaces synchronous oscillation as the dominant state. In  $R$  mode, the picture is qualitatively the same and we can compare simulation data (left inset) with experimental results [right inset Fig. 3(c)]. The experimental evolving trend of dissipation is accurately captured by simulations.

The results so far show that, between two possible states, the system favors the one with stronger dissipation. In this light, beating cilia coupled through a freely moving base, which supports breaststroke and freestyle synchrony at the

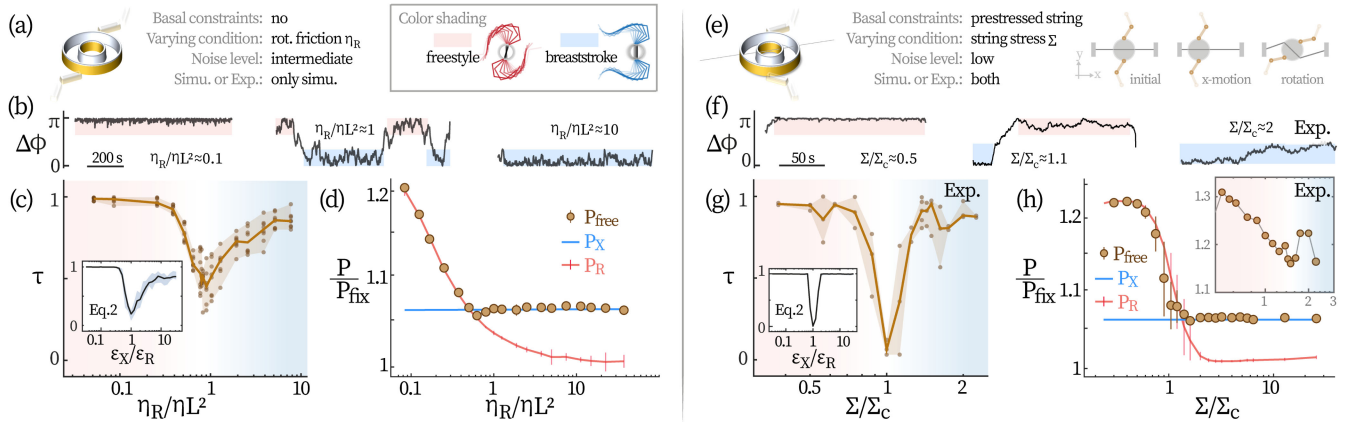


FIG. 4. Competition between the modes of synchrony. (a),(e) Schematic of the setup for two testing conditions. Drawing to the right of (e) displays how the elastic string modulates basal translation and rotation differently. (b),(f) Typical time series of ciliary phase difference  $\Delta\phi$  (folded to  $[0, \pi]$ ), demonstrating the transition from the freestyle ( $\Delta\phi \approx \pi$ , red shaded) to the breaststroke gait ( $\Delta\phi \approx 0$ , blue shaded). (c),(g) The systems’ total time fraction of synchrony  $\tau$ . Background colors indicate the dominant gait. Dots: single measurements; brown line and shading: median and interquartile. The insets are the predictions by the same generalized Adler equation, Eq. (2), with only different levels of noise to reproduce the observations in simulations and experiments. (d),(h) The systems’ total dissipative power when the base is free (circles), or geometrically constrained ( $R$  and  $X$  mode). Inset of (h): corresponding experimental data. Error bars: 1 std.  $P_{\text{fix}}$ : dissipation on a fixed base.

same time, could be directed into either mode by tuning the modes' relative dissipation. We now test this scenario with coupled cilia anchored on a free base [Figs. 4(a) and 4(e)].

In simulations, we fix  $\eta$  and hence keep the dissipation of breaststroke gait ( $P_X$ ) constant. Meanwhile,  $\eta_R$ , the friction coefficient for basal rotation, is decoupled from  $\eta$  and varied to modulate dissipation of freestyle gait ( $P_R$ ). Under given  $\eta_R$ ,  $P_R$  and  $P_X$  is measured by putting the system in  $R$  mode and  $X$  mode, respectively. Then, we free the base from any hard constraints, i.e., it can now simultaneously rotate and translate [Fig. 4(a)]. The system's actual dissipation with the free base is measured as  $P_{\text{free}}$ .

From left to right, Fig. 4(b) shows the breaststroke (blue) overtaking the freestyle (red) as the system's dominant gait under increasing  $\eta_R$  (nondimensionalized by  $\eta L^2$ ). Near the transition point, ciliary synchronization becomes less stable—as marked by the drop in total synchronized time fraction  $\tau$  [Fig. 4(c)]. Since  $\eta_R$  does not vary detuning, the destabilization must result from a decreased coupling strength, i.e., the presence of two possible gaits weakens the total coupling. This effect is captured by including the in-phase (IP) and antiphase (AP) coupling simultaneously into Eq. (1):

$$\Delta\dot{\phi} = 2\pi\nu - 2\pi\epsilon_X \sin \Delta\phi - 2\pi\epsilon_R \sin(\Delta\phi - \pi) + \zeta(t), \quad (2)$$

with  $\epsilon_X$  and  $\epsilon_R$  (both  $> 0$ ) the IP and AP coupling strengths, respectively. In this way, a free base provides an effective coupling of  $\epsilon_X - \epsilon_R$ , i.e., synchrony emerges when  $|\epsilon_X - \epsilon_R| > |\nu|$ . The equation reproduces the evolving trend of  $\tau$  ( $\epsilon_X = 2.5\nu$ ,  $T_\phi = 0.9$ ), see Fig. 4(c) inset. Finally, we benchmark the system's actual dissipation  $P_{\text{free}}$  against those under constraints,  $P_R$  and  $P_X$  [Fig. 4(d)]. Clearly, maximal dissipation is the underlying basis of gait competition.

Experimentally, it is challenging to decouple  $\eta_R$  from  $\eta$  and we thus employ another approach to modulate  $P_R$ . A prestressed elastic string is integrated into the base. In effect, the string's stress  $\Sigma$  limits basal rotation but not translation because translation does not induce further stretch while rotation does, see Fig. 4(e), SV 6 and [22]. Similar to increasing  $\eta_R$ , raising  $\Sigma$  also makes breaststroke the dominant gait [Fig. 4(f)]. We denote the critical stress where gait dominance changes as  $\Sigma_c$  and scale  $\Sigma$  with it. Near the transition,  $\tau$  drops more sharply than in Fig. 4(c), which attributes to a lower noise in experiments ( $T_\phi = 0.06$ ), see Fig. 4(g) and inset. With such a low noise, the system is rarely found to switch between gaits near the transition point. In simulations, systems with similar recovery torques also favor the more dissipative mode, see Fig. 4(h) main figure. The corresponding experimental data are displayed in the inset, aligning with the simulation trend.

*Discussion*—In overdamped systems, heat dissipation is related to the entropy production of the medium, which

corresponds to total entropy production in the stationary state [30,31]. Therefore, our finding, that the more dissipative state dominates, is in line with the maximum entropy production principle found in some other non-equilibrium dissipative systems [32]; and the present setup opens a new avenue for exploring the governing principle of nonequilibrium systems' evolution.

This study also has important implications for understanding the phase dynamics of biological biciliates. For example, our results provide a possible explanation to why wild-type CR only beats stably in breaststroke but not in freestyle: its ciliary basal connections may form a mesh that favors translation over rotation. Meanwhile, regarding the pending question why the CR mutant *ptx1* beats bistably in both breaststroke and freestyle gaits [15,28,33,34], we show that sufficient noise is needed. This aligns with recent observations [15] and advances our understanding of the role of noise in biological ciliary synchronization. Last, our finding provides an energetic perspective for understanding mode competition in biological ciliary synchronization in more complex scenarios.

*Acknowledgments*—We thank Xiangjun Xing for helpful discussions. This work was supported by the National Natural Science Foundation of China (No. T2325027, No. 12274448, No. 12174434, No. 11874395, No. 12074406, No. T2221001, No. 12204525), National Key R&D Program of China (2022YFF0503504), the Strategic Priority Research Program of Chinese Academy of Sciences (No. XDB33000000), and the China Postdoctoral Science Foundation (No. YJ20200202).

- 
- [1] A. Pikovsky, M. Rosenblum, and J. Kurths, *Synchronization: A Universal Concept in Nonlinear Sciences*, Cambridge Nonlinear Science Series (Cambridge University Press, Cambridge, England, 2001), [10.1017/CBO9780511755743](https://doi.org/10.1017/CBO9780511755743).
  - [2] D. Wei, P.G. Dehnavi, M.-E. Aubin-Tam, and D. Tam, *Phys. Rev. Lett.* **122**, 124502 (2019).
  - [3] D. Wei, P.G. Dehnavi, M.-E. Aubin-Tam, and D. Tam, *J. Fluid Mech.* **915**, A70 (2021).
  - [4] J. Elgeti, R. G. Winkler, and G. Gompper, *Rep. Prog. Phys.* **78**, 056601 (2015).
  - [5] J. Elgeti and G. Gompper, *Proc. Natl. Acad. Sci. U.S.A.* **110**, 4470 (2013).
  - [6] A. Vilfan and F. Jülicher, *Phys. Rev. Lett.* **96**, 058102 (2006).
  - [7] B. Guirao, A. Meunier, S. Mortaud, A. Aguilar, J.-M. Corsi, L. Strehl, Y. Hirota, A. Desoeuvre, C. Boutin, Y.-G. Han, Z. Mirzadeh, H. Cremer, M. Montcouquiol, K. Sawamoto, and N. Spassky, *Nat. Cell Biol.* **12**, 341 (2010).
  - [8] V.F. Geyer, F. Jülicher, J. Howard, and B.M. Friedrich, *Proc. Natl. Acad. Sci. U.S.A.* **110**, 18058 (2013).
  - [9] G.S. Klindt, C. Ruloff, C. Wagner, and B.M. Friedrich, *Phys. Rev. Lett.* **117**, 258101 (2016).

- [10] D. M. Woolley, R. F. Crockett, W. D. I. Groom, and S. G. Revell, *J. Exp. Biol.* **212**, 2215 (2009).
- [11] D. R. Brumley, K. Y. Wan, M. Polin, and R. E. Goldstein, *eLife* **3**, e02750 (2014).
- [12] N. Pellicciotta, E. Hamilton, J. Kotar, M. Faucourt, N. Delgehr, N. Spassky, and P. Cicuta, *Proc. Natl. Acad. Sci. U.S.A.* **117**, 8315 (2020).
- [13] G. Quaranta, M.-E. Aubin-Tam, and D. Tam, *Phys. Rev. Lett.* **115**, 238101 (2015).
- [14] K. Y. Wan and R. E. Goldstein, *Proc. Natl. Acad. Sci. U.S.A.* **113**, E2784 (2016).
- [15] D. Wei, G. Quaranta, M.-E. Aubin-Tam, and D. S. Tam, *eLife* **13**, e86102 (2024).
- [16] A. W. J. Soh, L. G. Woodhams, A. D. Junker, C. M. Enloe, B. E. Noren, A. Harned, C. J. Westlake, K. Narayan, J. S. Oakey, P. V. Bayly, and C. G. Pearson, *Mol. Biol. Cell* **33**, br18 (2022).
- [17] R. Kamiya and E. Hasegawa, *Exp. Cell Res.* **173**, 299 (1987).
- [18] E. Zheng, M. Brandenbourger, L. Robinet, P. Schall, E. Lerner, and C. Coulais, *Phys. Rev. Lett.* **130**, 178202 (2023).
- [19] O. Dauchot and V. Démery, *Phys. Rev. Lett.* **122**, 068002 (2019).
- [20] K. C. Leptos, K. Y. Wan, M. Polin, I. Tuval, A. I. Pesci, and R. E. Goldstein, *Phys. Rev. Lett.* **111**, 158101 (2013).
- [21] Hopf bifurcation is shown to underpin the emergence of spontaneous oscillation, which requires  $F_a/C$  to exceed a threshold, with  $C$  the stiffness of inter-Hexbug connection.
- Our setup represents the extreme case with zero elasticity ( $C = 0$ ) such that there is no threshold for activity ( $F_a$ ).
- [22] See Supplemental Material at <http://link.aps.org/supplemental/10.1103/PhysRevLett.133.048302>, which includes Refs. [23,24] for additional information about the experimental methods, extended simulation results, and a detailed discussion of the numerical simulations.
- [23] M. P. Allen and D. J. Tildesley, *Computer Simulation of Liquids* (Oxford University Press, New York, 1987).
- [24] M. Polin, I. Tuval, K. Drescher, J. P. Gollub, and R. E. Goldstein, *Science* **325**, 487 (2009).
- [25] B. Kralemann, L. Cimponeriu, M. Rosenblum, A. Pikovsky, and R. Mrowka, *Phys. Rev. E* **77**, 066205 (2008).
- [26] The frictional power for a rod-shaped object (length  $L$ ) rotating at angular speed  $\omega$  is  $\eta L^2 \omega^2 / 12$ . Writing the power in the form of  $\eta_R \omega^2$ , one obtains  $\eta_R / \eta = L^2 / 12$ .
- [27] U. Ruffer and W. Nultsch, *Cell Motil. Cytoskeleton* **7**, 87 (1987).
- [28] J. Horst and G. B. Witman, *J. Cell Biol.* **120**, 733 (1993).
- [29] Y. Izumida, H. Kori, and U. Seifert, *Phys. Rev. E* **94**, 052221 (2016).
- [30] U. Seifert, *Phys. Rev. Lett.* **95**, 040602 (2005).
- [31] U. Seifert, *Rep. Prog. Phys.* **75**, 126001 (2012).
- [32] L. Martyushev and V. Seleznev, *Phys. Rep.* **426**, 1 (2006).
- [33] Y. Liu, R. Claydon, M. Polin, and D. R. Brumley, *J. R. Soc. Interface* **15** (2018).
- [34] H. Guo, Y. Man, K. Y. Wan, and E. Kanso, *J. R. Soc. Interface* **18**, 20200660 (2021).